Homoclinic chaos in systems perturbed by weak Langevin noise

A. R. Bulsara
Research Branch, Naval Ocean Systems Center, San Diego, California 92152

W. C. Schieve
Physics Department and Ilya Prigogine Center for Studies in Statistical Mechanics, University of Texas, Austin, Texas 78712

E. W. Jacobs
Research Branch, Naval Ocean Systems Center, San Diego, California 92152
(Received 19 May 1989)

We consider the effect of weak additive noise on the homoclinic threshold of a driven dissipative nonlinear system. A new "generalized" Melnikov function is derived for the system and is seen to be the Melnikov function for the corresponding noise-free system plus a correction term that depends on the second-order noise characteristics. The correction term is explicitly calculated for three model systems [Duffing oscillator, Josephson junction, and rf superconducting quantum interference device (SQUID)]. The effect of a distribution of dc driving terms on the chaotic attractor of a dissipative system is also examined via numerical simulation of the rf SQUID.

I. INTRODUCTION

In this paper we wish to consider the appearance of homoclinic instabilities in driven classical nonlinear systems perturbed by weak external Langevin noise. For classical dissipative noise-free systems it has been well known since Poincaré[1] that, under perturbation, the stable and unstable manifolds emanating from a hyperbolic fixed point no longer coincide, and may intersect. The resulting complicated motion is an indication of the existence of chaos and, according to an existence theorem of Smale and Moser,[2] is homeomorphic to a Markov shift map. A simple theoretical test function due to Melnikov[3-6] may be used as a test of this homoclinic instability. This function, which measures the separation between the unstable and stable solution manifolds (the system parameters that cause the function to vanish correspond to the situation in which these manifolds touch), has been applied to a number of driven nonlinear oscillators [e.g., Duffing oscillator,[4-5] Josephson junction,[7-11] and rf superconducting quantum interference device[12] (SQUID)] with the aim of determining the set of system and driving parameters that lead to the onset of the homoclinic instability.

When one considers the onset of chaos in an actual (i.e., in the real world) system, the presence of noise in the external perturbation cannot be ruled out. Recently, a number of researchers have attempted to quantify the effect of weak external Langevin-type noise (such noise manifests itself in the system dynamics as an additive term in the external perturbation) on the transition to chaos in driven nonlinear systems. Early work on this problem was carried out by Crutchfield, Farmer, and Huberman,[13] who considered the effect of noise on period doubling in a discrete system. The noise was found to introduce a gap in the bifurcation sequence, which implied a scaling behavior at the chaotic threshold, in the critical exponents. Similar work was carried out by Svensmark and Samuelson[14] on the Josephson junction; they found that, in the presence of noise and a resonant external perturbation, the bifurcation point shifted by an amount proportional to the square of the perturbation amplitude. The amplification of a small resonant periodic perturbation in the presence of noise, near the period-doubling threshold, has also been investigated by Wiesenfeld and McNamara.[15,16] Arecchi, Badii, and Politi[17] have investigated the effect of noise on the forced Duffing oscillator in the region of parameter space where different chaotic attractors coexist, finding that the noise may lead to jumps between the different basins of attraction, with the noise-induced transitions obeying simple kinetic equations. Recent work, along the same lines, has been carried out by Kautz[18] on the problem of thermally induced escape from the basin of attraction in a dc-biased Josephson junction. The average escape time has been found to increase exponentially with inverse temperature, in the low-temperature limit. Finally, Kapitaniak[19] has investigated the behavior of the probability density function (obtained from the Fokker-Planck equation) of a dissipative nonlinear system driven by random and periodic forces. He finds that, for a choice of damping and deterministic parameters such that the noise-free system is chaotic, the stationary probability density function corresponding to the noisy case exhibits multiple maxima. Further, he defines a maximal Liapounov characteristic exponent in the presence of noise. This exponent is itself a random number with a corresponding probability density function. As the noise strength increases, the mean value of this exponent approaches zero. The averaged ex-

ponent is a smoother function of the system (and driving) parameters than its noise-free analog. This indicates that the noise may actually introduce a degree of order (or smoothing) in the chaotic system; a similar conclusion was obtained earlier by Matsumoto and Tsuda,[20] who considered the effect of noise on chaotic behavior in the Belousov-Zhabotinsky reaction.

In all the work cited in the preceding paragraph, the emphasis has been on the effect of external noise on either the period-doubling bifurcations that precede the appearance of chaotic attractors, or on the chaotic attractors themselves. No mention has been made of the effect of the noise on the homoclinic threshold as defined by the Melnikov function. The first calculation of such an effect was carried out by Schieve and Petrosky.[21,22] They considered the effect of noise on the homoclinic threshold in a classical system under the influence of zero-point quantum fluctuations. A new quantum-mechanical Melnikov function defined by them was found to consist of its classical counterpart shifted by a constant quantum correction, which was found to be simply the quantum energy fluctuation on the stable and unstable manifolds. Hence the classical homoclinic threshold was suppressed by the quantum noise; the quantum Melnikov function admitted of a zero in a different region of parameter space than its classical counterpart.

In this work, we consider a classical dissipative nonlinear system driven by a deterministic perturbing term, in the presence of weak external noise. A generalized Melnikov function for the noisy system is defined in Sec. II. This function may be written down as the Melnikov function in the corresponding noise-free problem, shifted by a constant correction term which takes into account the effect of the noise. In Sec. III we describe, formally, the procedure for calculating this correction term and the calculation is demonstrated, in Sec. IV, for three model nonlinear systems (Duffing oscillator, Josephson junction, and rf SQUID). The stochastic differential equation corresponding to the dissipative nonlinear problem (specifically, the rf SQUID) in the presence of random and periodic driving terms is numerically integrated in Sec. V. The noise is introduced by allowing the *initial* values of the random force to have a Gaussian distribution with specified variance (this is equivalent to introducing a random change in the system potential for each initial value) for each integration of the stochastic differential equation. In Sec. V we also consider the probability density function corresponding to the dependent variable in the nonlinear system dynamics. This function is found to have multiple maxima, and increasing the noise level has a smoothing effect on it. We also consider the probability density function corresponding to the generalized Melnikov function of Sec. II. This calculation provides a test of the accuracy of our theoretical computations (specifically, the noise-induced shift in the homoclinic threshold) of Secs. II–IV. Corresponding to our approach, Carlson[23,24] has investigated a shift map in the presence of thermal noise by means of an analogy to the eight-vertex model of spins. He has shown that the sequences corresponding to the homoclinic points of the Cantor set are removed by the noise.

II. GENERAL CASE: EFFECT OF WEAK ADDITIVE NOISE

Let us consider a general nonlinear second-order system driven by *weak* external additive noise. The state (e.g., displacement) variable $x(t)$ describing the evolution of this system is assumed to obey the dynamic equation (the dots denote differentiation with respect to time),

$$\ddot{x}+f(x)=F(t)\ , \tag{1}$$

where $F(t)$ is the random driving term which we take to be Gaussian, δ correlated with finite mean and variance σ^2

$$\langle F(t)\rangle=m,\quad \langle F(t)F(t+\tau)\rangle=\sigma^2\delta(\tau)\ , \tag{2}$$

$\delta(\tau)$ being the Dirac δ function. $f(x)$ is a nonlinear function of the dynamic variable $x(t)$. In the absence of the random force, the system (1) is conservative and represents a particle moving in a potential $U(x)\equiv\int^x f(y)dy$.

We now introduce, as perturbations, a dissipative term $-k\dot{x}$ and a deterministic (often taken to be periodic) driving term $Qg(t,t_0)$ on the right-hand side of (1). In the absence of the random force $F(t)$, the introduction of these perturbations is known to induce homoclinic behavior in the system for certain sets of values of the system and driving parameters. This behavior is characterized by a bifurcation of the separatrix (i.e., unperturbed) solution into stable and unstable solution manifolds. The small separation of these manifolds is given by the Melnikov function. When this function vanishes, the manifolds touch and above this threshold one may (for certain values of the system and driving parameters) observe chaotic behavior characterized by the appearance of strange attracting sets in phase space. The Melnikov function is given (for the noise-free system) by[3–6]

$$\Delta(t_0)=-k\int_{-\infty}^{\infty}\dot{x}_s^2(t)dt+Q\int_{-\infty}^{\infty}\dot{x}_s(t)g(t,t_0)dt\ . \tag{3}$$

Here $x_s(t)$ represents the separatrix (or unperturbed) solution, i.e., the solution of (1) in the absence of any dissipative or driving terms.

In the presence of noise, the formalism of the preceding paragraph must be modified. Let us return to the noise-driven equation (1) and treat this as our "unperturbed" system. The solution $x(t)$ of (1) may be expressed as the separatrix solution plus a (small) noise-induced deviation

$$x(t)=x_s(t)+\delta x(t)\ , \tag{4}$$

with a similar expression holding for the velocity $\dot{x}(t)$. Averaging over the ensemble of the random force yields for the mean displacement

$$\langle x(t)\rangle=x_s(t)+\langle\delta x(t)\rangle\ , \tag{5}$$

where the angular brackets denote an average over the ensemble of $F(t)$ and a similar expression holds true for the averaged velocity $\langle\dot{x}(t)\rangle$. We now substitute the expansion (4) into (1), expand to leading order in δx, and separate out the terms that depend on the random force

$F(t)$. The result is the two equations

$$\ddot{x}_s + f(x_s) = 0 , \tag{6a}$$

$$\delta\ddot{x} - \omega^2(t)\delta x = F(t) . \tag{6b}$$

Here $\omega^2(t) \equiv -[df(x)/dx]_{x=x_s}$ is, in general, a complicated function of time due to the time dependence of the separatrix solution $x_s(t)$. Equation (6a) describes the unperturbed motion, i.e., the separatrix. Its solution may be obtained for specific forms of the function $f(x_s)$. Equation (6b) yields the stochastic component of the solution to the unperturbed problem (1). In its present form, it cannot be integrated (except numerically). We shall see, however, that the corrections to the Melnikov integral require us to compute the *averaged* quantities $\langle \delta\dot{x}(t) \rangle$ and $\langle \delta\dot{x}^2(t) \rangle$. These quantities may be computed using a procedure that will be described in Sec. III.

We now introduce a Melnikov function in the presence of the random force. This function defines the separation of the stable and unstable manifolds for each realization of the weak random force term $F(t)$ and may be written as

$$\Delta_F(t_0) = -k \int_{-\infty}^{\infty} \dot{x}^2(t) dt + Q \int_{-\infty}^{\infty} \dot{x}(t) g(t, t_0) dt , \tag{7}$$

Recalling that we have treated the noise system (1) as our unperturbed system, the analogy between (7) and the usual definition of the Melnikov function (3) is evident. One readily observes that (7) may be cast in the form

$$\Delta_F(t_0) = \Delta(t_0) + \Delta_c(t_0) , \tag{8}$$

where Δ_c is a correction term. The Melnikov function Δ_F defined in (8) is a random variable, since the correction Δ_c involves the stochastic component $\delta\dot{x}(t)$ of the velocity. One observes that the homoclinic threshold is shifted for each element of the stochastic ensemble: the zeros of (8) do not coincide with those of (3). One may first obtain an expression for its *average* value by averaging (8) over the ensemble of the random force. In this case, we obtain the averaged Melnikov function

$$\langle \Delta_F(t_0) \rangle = \Delta(t_0) + \langle \Delta_c(t_0) \rangle , \tag{9}$$

where the averaged correction is given [using (4)] by

$$\begin{aligned} \langle \Delta_c(t_0) \rangle \equiv & -2k \int_{-\infty}^{\infty} \dot{x}_s(t) \langle \delta\dot{x}(t) \rangle dt \\ & + Q \int_{-\infty}^{\infty} g(t, t_0) \langle \delta\dot{x}(t) \rangle dt \\ & - k \int_{-\infty}^{\infty} \langle \delta\dot{x}^2(t) \rangle dt . \end{aligned} \tag{10}$$

The ensemble-averaged Melnikov function defined in (10) is a generalization of the usual function (3) defined in connection with the noise-free problem. It is similar to the function introduced by Schieve and Petrosky[21-22] to take into account the effects of small quantum fluctuations on the homoclinic threshold in a classical nonlinear system. The terms appearing on the right-hand side of (10) may be computed for specific model systems. In the following section we describe the calculation in general. This is followed by a computation of the correction term for specific systems. Before moving on, however, we wish to point out that a significant and formidable question exists regarding the existence of a Smale-Birkoff theorem[5] for solutions to the stochastic differential equation (1). Our work here and in the following sections suggests that under weak noise there are, following the noisy tangency, multiple crossings for each realization of the ensemble and thus a Cantor-set-like structure in this weak sense.

III. COMPUTATION OF $\langle \Delta_c(t_0) \rangle$: THE NOISE CORRECTION TO THE MELNIKOV FUNCTION

We now consider the computation of the mean value $\langle \delta\dot{x}(t) \rangle$ and the second-order correlation function $\langle \delta\dot{x}^2(t) \rangle$ appearing in (10). To do this, we employ a stochastic description in which the stochastic differential equation (6b) is replaced by a linear inhomogeneous Fokker-Planck or diffusion equation[25] for the probability density function $P(\delta x, \delta\dot{x}, t | \delta x(t_0), \delta\dot{x}(t_0), t_0)$ corresponding to the random variables $\delta x(t)$ and $\delta\dot{x}(t)$. The probability density function, as well as the second-order correlation function, may be obtained in closed form from this Fokker-Planck equation once the solutions for $\langle \delta x(t) \rangle$ and $\langle \delta\dot{x}(t) \rangle$ are known. The procedure has been outlined by van Kampen,[26] whose treatment and notation we follow in the remainder of this section.

We first consider the case when the random force term $F(t)$ has zero mean value, i.e., $m = 0$. Then, the stochastic differential equation (6b) leads one to a two-dimensional Fokker-Planck equation for the probability density function $P(\underline{y}, t)$

$$\frac{\partial P}{\partial t} = -\sum_{ij} A_{ij} \frac{\partial}{\partial y_j} y_i P + \frac{\sigma^2}{2} \sum_{ij} B_{ij} \frac{\partial^2 P}{\partial y_i \partial y_j} , \tag{11}$$

where we have defined the matrices,

$$\begin{aligned} \underline{y}(t) &\equiv \begin{bmatrix} \delta x(t) \\ \delta\dot{x}(t) \end{bmatrix} , \\ \underline{A}(t) &\equiv \begin{bmatrix} 0 & 1 \\ \omega^2(t) & 0 \end{bmatrix} , \\ \underline{B} &\equiv \begin{bmatrix} 0 & 0 \\ 0 & 1 \end{bmatrix} . \end{aligned} \tag{12}$$

In order to obtain the solution of (11), we must first solve the transport equation [obtained by averaging the stochastic differential equation (6b) over the ensemble of the random force $F(t)$]

$$\frac{d^2}{dt^2} \langle \delta x(t) \rangle = \omega^2(t) \langle \delta x(t) \rangle . \tag{13}$$

In terms of the matrix $\underline{y}(t)$ defined in (12), the formal solution of (13) may be written down in the form

$$\langle \underline{y}(t) \rangle = \underline{Y}(t) \langle \underline{y}(t_0) \rangle , \tag{14}$$

$\underline{Y}(t)$ being the Green's function determined by

$$\dot{\underline{Y}}(t) = \underline{A}(t) \underline{Y}(t), \quad \underline{Y}(t_0) = 1 . \tag{15}$$

We shall return to a precise computation of the elements

of $\underline{Y}(t)$ later in this section. We define the correlation matrix $\underline{\Sigma}(t)$ by

$$\Sigma_{ij} \equiv \langle y_i y_j \rangle - \langle y_i \rangle \langle y_j \rangle \ . \tag{16}$$

It obeys the matrix differential equation

$$\dot{\underline{\Sigma}}(t) = \underline{A}\underline{\Sigma} + \underline{\Sigma}\,\underline{\tilde{A}} + \sigma^2 \underline{B} \ , \tag{17}$$

where $\underline{\tilde{A}}$ is the transpose of $\underline{A}$. The solution of (17) may be formally written down [in terms of an initial correlation matrix $\underline{\Sigma}(t_0)$] as

$$\underline{\Sigma}(t) = \underline{Y}(t)\underline{\Sigma}(t_0)\underline{\tilde{Y}}(t) + \sigma^2 \int_{t_0}^{t} \underline{Y}(t)\underline{Y}(t')^{-1}\underline{B}(t')\underline{\tilde{Y}}(t')^{-1}\underline{\tilde{Y}}(t)dt' \ , \tag{18}$$

and the probability density function $P(\underline{y},t)$ appearing in the Fokker-Planck equation (11) takes the form

$$P(\underline{y},t) = (4\pi^2 \det \underline{\Sigma})^{-1/2} \times \exp[-\tfrac{1}{2}(\underline{\tilde{y}} - \langle \underline{\tilde{y}} \rangle)\underline{\Sigma}^{-1}(\underline{y} - \langle \underline{y} \rangle)] \ . \tag{19}$$

Using (16) and (18), we readily obtain

$$\langle \delta\dot{x}^{\,2}(t) \rangle = \langle \delta\dot{x}(t) \rangle^2 + [\underline{Y}(t)\underline{\Sigma}(t_0)\underline{\tilde{Y}}(t)]_{22} + \sigma^2 \int_{t_0}^{t} K_{22}(t,t')dt' \ , \tag{20}$$

where we have set $\underline{K}(t,t') \equiv \underline{Y}(t)Y(t')^{-1}\underline{B}\underline{\tilde{Y}}(t')^{-1}\underline{\tilde{Y}}(t)$, the kernel of the integral appearing on the right-hand side of (18). In addition to the matrix element $K_{22}(t,t')$, the expression (20) includes the initial variances defined by

$$\begin{aligned} \Sigma_{11}(t_0) &= \langle \delta x^2(t_0) \rangle , \\ \Sigma_{12}(t_0) &= \langle \delta x(t_0)\delta\dot{x}(t_0) \rangle \ , \\ \Sigma_{21}(t_0) &= \langle \delta\dot{x}(t_0)\delta x(t_0) \rangle \ , \\ \Sigma_{22}(t_0) &= \langle \delta\dot{x}^{\,2}(t_0) \rangle \ . \end{aligned} \tag{21}$$

It remains to evaluate the averaged solution $\langle \delta\dot{x}(t) \rangle$ as well as the matrix $\underline{Y}(t)$ in terms of the parameters appearing in our original stochastic differential equation (6b). We now demonstrate how this is done.

Let us return to the transport equation (13). This equation is to be solved for the average value $\langle \delta x(t) \rangle$, usually using a WKB technique [since $\omega^2(t)$ is, in general, a complicated function of time]. The precise form of the solution will depend on the model system under consideration (this will be discussed in greater detail in Sec. IV when we apply our results to three specific model systems). Let us assume, for the time being, that the function $\omega^2(t)$ admits of only one turning point (i.e., it changes sign only once) in the range $0 \le t \le \infty$. Then, one may write down a general solution to (13) in the form

$$\langle \delta x(t) \rangle = C_1 f_1(t) + C_2 f_2(t) \ , \tag{22}$$

where $C_{1,2}$ are integration constants (to be determined by the boundary or initial conditions). The function $f_1(t)$ is given by[27]

$$f_1(t) = S_0^{1/6}[\omega^2(t)]^{-1/4}\mathrm{Ai}[(\tfrac{3}{2}S_0)^{2/3}] \ , \tag{23}$$

where

$$S_0(t) \equiv \int_{t_c}^{t} \omega(t')dt' \ , \tag{24}$$

and Ai is the Airy function. t_c is the turning point of $\omega^2(t)$, i.e., $\omega^2(t_c)=0$. The other part $f_2(t)$ of the solution is found, using standard techniques, to be

$$f_2(t) = f_1(t)\int_{t_0}^{t} \frac{dt'}{f_1^2(t')} \ . \tag{25}$$

Once again we emphasize that the precise behavior of these solutions (e.g., at long times) depends on the system under consideration, through the function $\omega^2(t)$ and that the equations (23)–(25) are true under the assumption that the function $\omega^2(t)$ has just one turning point in the interval $0 \le t \le \infty$. In such cases, the solution $f_1(t)$ generally represents the solution that converges in the $t \to \infty$ limit, whereas $f_2(t)$ diverges in this limit. In fact, one may break up the general solution (23) into distinct solutions for $t < t_c$ and $t > t_c$. These solutions are to be "patched" together in the connection region $t \approx t_c$. For this procedure to hold, i.e., for (23) to represent a unified solution for all $t > 0$, the condition[27]

$$\left| \frac{d}{dt}\omega^2(t_c) \right|^{4/3} \gg \left| \frac{d^2}{dt^2}\omega^2(t_c) \right| \ , \tag{26}$$

must be satisfied. Then the unified solution (23) may be written down in terms of three distinct solutions[27]

$$\begin{aligned} f_1(t) &= 2\sqrt{\pi}\frac{(\frac{3}{2}S_0)^{1/6}}{|\omega^2(t)|^{1/4}}\mathrm{Ai}[(\tfrac{3}{2}S_0)^{2/3}] \approx [\omega^2(t)]^{-1/4}\exp\left[-\int_{t_c}^{t}\omega(t')dt'\right], \quad t > t_c \\ &= 2\sqrt{\pi}\frac{(\frac{3}{2}S_0)^{1/6}}{|\omega^2(t)|^{1/4}}\mathrm{Ai}[-(\tfrac{3}{2}S_0)^{2/3}] \approx [-\omega^2(t)]^{-1/4}\sin\left[\int_{0}^{t_c}[-\omega^2(t)]^{1/2}dt\right], \quad 0 \le t \le t_c \\ &= 2\sqrt{\pi}\left[\frac{3}{2d\omega^2(t_c)/dt}\right]^{1/6}\mathrm{Ai}\left\{\left[\tfrac{3}{2}t_c^{3/2}\left[\frac{d}{dt}\omega^2(t_c)\right]^{1/2}\right]^{2/3}\right\}, \quad t \approx t_c \ . \end{aligned} \tag{27}$$

The constants $C_{1,2}$ are now determined. Assuming that both $\langle \delta x(t) \rangle$ and $\langle \delta\dot{x}(t) \rangle$ are initially nonzero, we readily find

$$f_2(t_0) = 0, \quad \dot{f}_2(t_0) = f_1^{-1}(t_0) \ , \tag{28a}$$

which leads to the expressions

$$\begin{aligned} C_1 &= \frac{\langle \delta x(t_0) \rangle}{f_1(t_0)} \ , \\ C_2 &= \langle \delta\dot{x}(t_0) \rangle f_1(t_0) - \langle \delta x(t_0) \rangle \dot{f}_1(t_0) \ . \end{aligned} \tag{28b}$$

Throughout this work we shall assume that $\langle \delta x(t_0)\rangle = 0 = \langle \delta \dot{x}(t_0)\rangle$; it then follows that $\langle \delta x(t)\rangle = 0 = \langle \delta \dot{x}(t)\rangle$ for all subsequent times t (for the $m=0$ case being currently considered). In this case, the averaged Melnikov correction term $\langle \Delta_c(t_0)\rangle$ involves only the second-order velocity correlation function $\langle \delta \dot{x}^2(t)\rangle$, in agreement with earlier calculations[21-22] on the effects of zero-point quantum fluctuations on classical chaotic systems. The above special initial conditions assume physically that, at time $t=t_0$, the *mean* displacement in the noisy unperturbed system follows the separatrix motion of the corresponding noise-free system. This condition ensures that the mean displacement follows the noise-free separatrix motion for all subsequent times as well.

The solution (22) [with $f_{1,2}(t)$ given by (23) and (25)] represents the solution of the *initial* value problem. In keeping with our fundamental assumption of weak noise, however, the problem must be solved as a *boundary* value problem with the requirement that both $\langle \delta x(t)\rangle$ and $\langle \delta \dot{x}(t)\rangle$ be finite as $t \to \infty$. In fact, we expect these quantities to follow qualitatively similar behavior to the corresponding separatrix quantities $x_s(t)$ and $\dot{x}_s(t)$, which implies that $\langle \delta \dot{x}(t_f)\rangle \to 0$ at some final time $t_f \to \infty$. Imposing these boundary conditions on the solution (22) and noting that $\dot{f}_1(t_f)/\dot{f}_2(t_f) \ll 1$ in the large t_f limit, one obtains, after some calculation, the solution of the boundary problem. This solution is diagonal,

$$\langle \delta x(t)\rangle = \frac{\langle \delta x(t_0)\rangle}{f_1(t_0)} f_1(t) ,$$
$$\langle \delta \dot{x}(t)\rangle = \frac{\langle \delta \dot{x}(t_0)\rangle}{\dot{f}_1(t_0)} \dot{f}_1(t) , \tag{29}$$

and involves the implicit constraint

$$\langle \delta \dot{x}(t_0)\rangle f_1(t_0) = \langle \delta x(t_0)\rangle \dot{f}_1(t_0) , \tag{30}$$

implying that, given an arbitrary initial displacement $\langle \delta x(t_0)\rangle$, the boundary condition requires that the initial velocity perturbation be determined by the above constraint. Note that the constraint (30) is equivalent to setting the constant C_2 defined in (28b), equal to zero.

In terms of the solution (29) we readily obtain for the elements of the matrix $\underline{K}(t,t')$

$$K_{11}(t,t') = 0 = K_{12}(t,t') = K_{21}(t,t') ,$$
$$K_{22}(t,t') = \frac{\dot{f}_1^2(t)}{\dot{f}_1^2(t')} . \tag{31}$$

The expression (31) together with the initial condition $\langle \delta x(t_0)\rangle = 0 = \langle \delta \dot{x}(t_0)\rangle$ [note that this condition is a special case of the constraint (30)] permits one to evaluate the mean correction term $\langle \Delta_c(t_0)\rangle$ defined in (10). The correction term is seen [from (20)] to depend solely on second-order fluctuations. In addition, one readily observes from (31) that, after carrying out the t' integration in (18), the resulting term is an odd function of t. Hence this term does not contribute to the integral appearing in the third term on the right-hand side of (10) and one obtains finally the relatively simple expression

$$\langle \Delta_c \rangle = -2k \frac{\langle \delta \dot{x}^2(0)\rangle}{\dot{f}_1^2(0)} \int_0^\infty \dot{f}_1^2(t) dt , \tag{32}$$

for the correction term. The above result has been obtained from the initial variance term in (31) with t_0 set equal to zero for convenience.

Before proceeding further, we pause to comment briefly on the assumption of weak Langevin noise. Throughout this work, the noise has been assumed to be sufficiently weak that the resulting motion (in the presence of the noise, but in the absence of the dissipative and deterministic forcing terms) is not appreciably different from the separatrix motion in the noise-free case. This permits one to carry out the expansion leading to (6a) and (6b) to first order and also ensures that the system does not make excursions to neighboring wells of the potential under the influence of the noise alone (this would be the case for very strong noise). Under these conditions, one may also assume that *at initial times*, the random variables $x(0)$ and $\dot{x}(0)$ [these variables refer to the solution of (1), i.e., the right-hand side of (4)] obey a joint probability density which may be assumed to be Gibbsian:

$$P(x(0),\dot{x}(0)) \equiv N^{-1} \exp(-2E/\sigma^2) , \tag{33}$$

where N is a normalization constant and E the total energy given by $E = \frac{1}{2}\dot{x}^2(0) + U(x(0))$. One readily obtains the initial velocity correlation function from (33)

$$\langle \dot{x}^2(0)\rangle \equiv N^{-1} \int_{-\infty}^{\infty} \dot{x}^2(0) P(x(0),\dot{x}(0)) dx(0) d\dot{x}(0) . \tag{34}$$

Since $\dot{x}_s(0) \equiv 0$ one readily obtains from (4) and (34)

$$\langle \delta \dot{x}^2(0)\rangle \equiv \langle \dot{x}^2(0)\rangle = \frac{\sigma^2}{2} . \tag{35}$$

The above result enables us to express the initial variance $\langle \delta \dot{x}^2(0)\rangle$ directly in terms of the noise variance. One may now set an *approximate* upper bound on the noise strength by requiring that the variance $\langle \delta \dot{x}^2(0)\rangle$ of the initial velocity perturbation be much smaller than the depth of the potential well. This ensures that the noise variance σ^2 is also much smaller than the well depth and allows us to quantify the assumption of "weak Langevin noise."

Returning to our discussion (32) for the Melnikov correction term, we see that, on average, the homoclinic threshold has been shifted from its parameter-space location in the corresponding noise-free case by an amount proportional to the variance of the noise. Indeed, setting $\langle \Delta_F \rangle = 0$ in (9) one readily obtains the new ratio Q/k of the perturbation amplitudes corresponding to the homoclinic threshold. The result may be written in the form

$$\frac{Q}{k} = A + B\sigma^2 , \tag{36}$$

where we have defined

$$A \equiv \left[\frac{Q}{k} \right]_0 , \tag{37}$$

and

$$B \equiv \frac{C}{\int_{-\infty}^{\infty} \dot{x}_s(t) g(t,t_0) dt} , \tag{38a}$$

$$C \equiv \frac{1}{2\dot{f}_1^2(0)} \int_{-\infty}^{\infty} \dot{f}_1^2(t) dt , \tag{38b}$$

where we have used (32) and (35). The quantity A defined in (37) represents the threshold ratio of Q/k in the noise-free system; it is obtained by setting the right-hand side of (3) equal to zero. The second term on the right-hand side of (36) represents the correction induced by the Langevin noise. Note that this term is always positive; the noise always *elevates* the homoclinic threshold.

We now consider briefly the case when the random driving term has a finite mean value m which now appears on the right-hand side of the transport equation (13). Using the initial conditions $\langle \delta x(0) \rangle = 0 = \langle \delta \dot{x}(0) \rangle$ as before, one may write down the solution of the transport equation in the form

$$\begin{aligned} \langle \delta x(t) \rangle &= m f(t) , \\ \langle \delta \dot{x}(t) \rangle &= m \dot{f}(t) , \end{aligned} \tag{39}$$

in terms of an undetermined function $f(t)$. One readily observes that, within the framework of our perturbation theory of Sec. II [the mean value m must be small and positive so that $\langle \delta x(t) \rangle \ll x_s(t)$ and $\langle \delta \dot{x}(t) \rangle \ll \dot{x}_s(t)$], the dominant contribution to the correction term (10) arises from the first two terms on the right-hand side of (10). One may verify that the absolute magnitude of the first term on the right-hand side of (10) is greater than or equal to that of the second term [for unit Q and k and for the case when $g(t,t_0)$ is an alternating periodic signal of the form to be considered in this work]. Hence the homoclinic threshold will always be elevated (or, at worst, stay the same) when the noise is assumed to have a finite mean value. In fact, one readily obtains for the threshold ratio Q/k corresponding to this case:

$$\begin{aligned} \frac{Q}{k} &= \left[\int_{-\infty}^{\infty} \dot{x}_s^2(t) dt + 2m \int_{-\infty}^{\infty} \dot{x}_s(t) \dot{f}(t) dt \right] \Big/ \left[\int_{-\infty}^{\infty} \dot{x}_s(t) g(t,t_0) dt + m \int_{-\infty}^{\infty} \dot{f}(t) g(t,t_0) dt \right] , \\ &\approx \left[\frac{Q}{k} \right]_0 \left[1 + 2m \left[\int_{-\infty}^{\infty} \dot{x}_s(t) \dot{f}(t) dt \Big/ \int_{-\infty}^{\infty} \dot{x}_s^2(t) dt \right] - m \left[\int_{-\infty}^{\infty} \dot{f}(t) g(t,t_0) dt \Big/ \int_{-\infty}^{\infty} \dot{x}_s(t) g(t,t_0) dt \right] \right] . \end{aligned} \tag{40}$$

The preceding remarks imply that one always has $(Q/k) \geq (Q/k)_0$ so that the presence of a finite mean value in the random term can never, of its own accord, induce homoclinic behavior.

In the following section, the theory presented so far is elucidated numerically in the case of three well-known model systems. We confine ourselves to the $m=0$ case, the important point being that the Langevin noise suppresses the observation of homoclinic chaos, in qualitative agreement with the work of Carlson.[23-24]

IV. EXAMPLES

In this section, we consider three well-known nonlinear problems: the Duffing oscillator, Josephson junction, and rf SQUID. In all three cases, we assume that the system is perturbed by a dissipative term $-k\dot{x}$ and a deterministic term $g(t,t_0)$, which we take to be periodic. In the presence of weak Langevin noise, the correction term $\langle \Delta_c \rangle$ is obtained using the WKB solutions (27) and (29), as well as by direct numerical integration of the transport equation (13). The agreement between the correction terms obtained using these two procedures is seen to be extremely good. Since the calculations are qualitatively similar for all three models, we first present the salient features of each model before computing the Melnikov function in each case in the presence of weak Langevin noise having zero mean and variance σ^2.

A. Duffing oscillator

We consider the Duffing oscillator with negative stiffness (sometimes referred to as the anti-Duffing oscillator).[4-5] The dynamic equations on the separatrix are

$$\begin{aligned} \dot{x} &= v \\ \dot{v} &= \beta x - \alpha x^3 . \end{aligned} \tag{41}$$

The above system is seen to be homologous to a particle moving in a potential given by

$$U(x) = -\frac{\beta x^2}{2} + \frac{\alpha x^4}{4} . \tag{42}$$

This potential (we assume $\beta = 1.0 = \alpha$ throughout this section) admits of a saddle point at $(x,v)=(0,0)$ and elliptic points at $(\pm 1,0)$. The particular unperturbed (or separatrix) solution is found by solving (41)

$$x_s(t) = \sqrt{2}\,\mathrm{sech}\, t . \tag{43}$$

We now introduce weak Langevin noise. Using the procedure of Sec. II we readily set up the transport equation (13) for the mean value $\langle \delta x(t) \rangle$ with $\omega^2(t)$ given by

$$\omega^2(t) = 1 - 6\,\mathrm{sech}^2 t . \tag{44}$$

This function is symmetric about $t=0$ and has a single turning point (for positive t) at $t_c = \mathrm{sech}^{-1}(1/\sqrt{6})$.

B. Josephson junction

The separatrix response of a Josephson junction may be written in the form[28]

$$\begin{aligned} \dot{x} &= v \\ \dot{v} &= -\beta \sin x , \end{aligned} \tag{45}$$

where k and β may be expressed in terms of the junction parameters and x is typically the phase of the supercurrent in the junction [it should be noted that (45) also describes the dynamics of a common pendulum in the absence of the small oscillation assumption]. Equation (45) may be derived from a potential

$$U(x)=-\beta\cos x \ . \tag{46}$$

One readily observes that this potential is periodic and has saddle points at $x=n\pi$ (n odd) with elliptic points at $x=2n\pi$. The separatrix solution may be found by solving (45)

$$x_s(t)=4\tan^{-1}(e^{\sqrt{\beta}t})+\pi \ . \tag{47}$$

Introducing noise as in the preceding example, we find for this case

$$\omega^2(t)=-2\beta^{3/2}\cos x_s(t)\,\mathrm{sech}(\sqrt{\beta}t) \ . \tag{48}$$

This function shows the same qualitative features as (44) and is not plotted. One readily obtains its turning point (for positive time) at $t_c=(1/\sqrt{\beta})\ln(\tan\frac{3}{8}\pi)$.

C. rf SQUID

In its simplest form, the rf SQUID consists of a single Josephson junction shorted by a superconducting loop. An external magnetic field produces a geometrical magnetic flux across the loop together with a circulating supercurrent in the loop. Hence the flux actually sensed by the SQUID is not the same as the original magnetic flux (the SQUID actually amplifies this flux because of the additional supercurrent induced in the loop by the Josephson tunneling current). The net flux is inductively coupled to a rf-driven detector cirvuit. Setting $x(t)$ equal to the flux sensed by the SQUID (in units of the universal flux quantum), the separatrix dynamics of the SQUID are given by[28]

$$\begin{aligned}\dot{x}&=v\\ \dot{v}&=-\omega_0^2 x-\beta\sin 2\pi x \ ,\end{aligned} \tag{49}$$

where, one again, the parameters β and ω_0^2 may be expressed in terms of the SQUID parameters. Homoclinic chaos in the rf SQUID has been treated in detail in Ref. 12. As with the formalism of Ref. 12, we transform to a new variable $z=2\pi x-\pi/2$ in terms of which one may consider the system (49) from the standpoint of a particle moving in a potential,

$$U(z)=\frac{\omega_0^2}{2}\left[z+\frac{\pi}{2}\right]^2+2\pi\beta\omega_0^2\sin z \ . \tag{50}$$

The potential is multistable above the critical value of the nonlinearity β and is plotted in Fig. 1 for $(\beta,\omega_0)=(2.0,1.0)$. In the remainder of this section, we shall confine our attention to the separatrix z_1z_2 in Fig. 1. This renders the rf SQUID qualitatively similar to the Duffing oscillator problem discussed above (note that had we considered the separatrix z_1z_3 in Fig. 1, the problem would have resembled the Josephson junction). For the case of moderate β this separatrix solution has been obtained as[12]

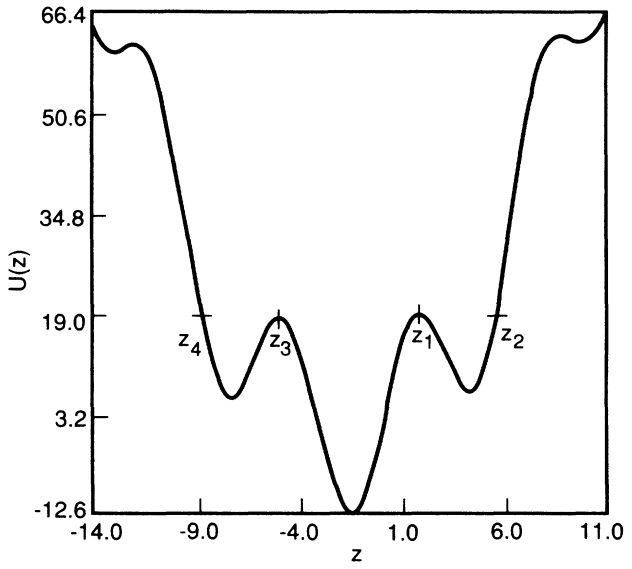

FIG. 1. Potential $U(z)$ [Eq. (50)] for the rf SQUID corresponding to $(\beta,\omega_0)\equiv(2.0,1.0)$.

$$z_s(t)=z_i-\alpha\tanh^2\zeta t \ , \tag{51}$$

where $\alpha=z_2-z_1$ and $\zeta=(0.1482\pi\beta\omega_0^2)^{1/2}$. Introducing noise as before, we readily obtain

$$\omega^2(t)=2\pi\beta\sin z_s(t)-1 \ , \tag{52}$$

Again, $\omega^2(t)$ is symmetric about $t=0$ and has a single turning point (for $t>0$) at

$$t_c=\zeta^{-1}\tanh^{-1}\left\{\frac{[z_2-\pi+\sin^{-1}(1/2\pi\beta)]}{\alpha}\right\}^{1/2} \ .$$

D. Results

We now assume that each of the above model systems is perturbed by a dissipative term $-k\dot{x}$ and a deterministic driving term which we take to be periodic: $g(t,t_0)\equiv Q\cos[\Omega(t+t_0)]$. Then, for the Duffing oscillator, the Melnikov function for the noise-free case is[4-5]

$$\Delta_D(t_0)=-\frac{4k}{3}+\sqrt{2}\pi\Omega Q(\sin\Omega t_0)\,\mathrm{sech}\frac{\pi\Omega}{2} \ . \tag{53}$$

The zero of this function (taken in units of $\sin\Omega t_0$) yields the homoclinic threshold in the absence of noise, but in the presence of the dissipative and deterministic driving terms. It is plotted in Fig. 2. The curve represents the second term (53) (in units of $\sin\Omega t_0$). It is peaked at a critical frequency $\Omega_{Dc}=2.399/\pi$. The straight line represents the absolute value of the first term. The values $(Q,k)\equiv(1.25,2.81)$ are used in these plots. This represents the threshold case; the straight line is tangential to the curve. We now assume that weak Langevin noise of variance $\sigma^2=0.2$ (corresponding to an initial velocity variance $\langle\delta\dot{x}^2(0)\rangle=0.1$) is present in the system.

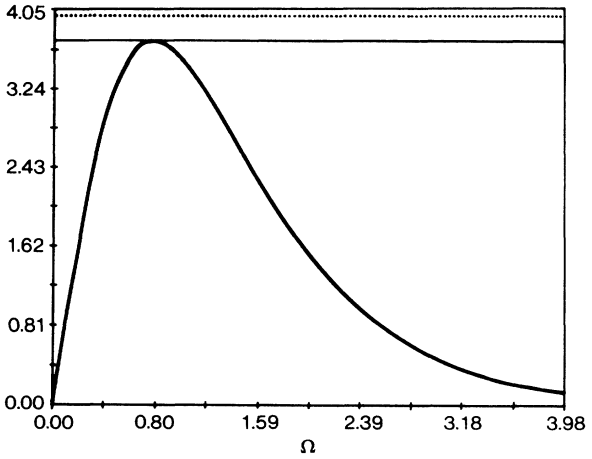

FIG. 2. Melnikov function for the Duffing oscillator. Solid curve represents the second term in (51) (in units of $\sin\Omega t_0$) for $Q=2.0$; solid line represents the first term in (53) for $k=2.81$ (threshold case). Dotted line represents the effect, on the straight line, of including noise of variance $\sigma^2=0.2$; it includes the correction $\langle \Delta_c \rangle$ calculated using the WKB approximation (29).

This leads to an elevation in the homoclinic threshold characterized by a displacement of the straight line in Fig. 2. One may also compute the displaced straight line through a direct numerical integration of the transport equation (11). The relative difference between the corrections is approximately 2.2% for this case.

The corresponding figure for the Josephson junction is readily obtained. The Melnikov function in the absence of noise is[7–10]

$$\Delta_J(t_0)=-8k\sqrt{\beta}+2\pi Q(\cos\Omega t_0)\operatorname{sech}\left[\frac{\pi\Omega}{2\sqrt{\beta}}\right], \quad (54)$$

which we plot in Fig. 3 for $(Q,k)=(2,1.57)$ corresponding to the homoclinic threshold (we set $\beta=1$ throughout). As in the preceding case, the curve represents the second term in (54) (in units of $\cos\Omega t_0$) and the straight line represents the first term. The curve is peaked at $\Omega_{Jc}=0$ because of the difference in parity of the separatrix velocity $\dot{x}_s(t)$ between this example and the Duffing oscillator. Once again, the introduction of noise with variance $\sigma^2=0.2$ leads to an elevation of the homoclinic threshold. The displaced line is plotted in the figure; its location differs from the position computed via numerical integration of the transport equation (11) by approximately 1% in this case.

Finally, we present, in Fig. 4, the Melnikov function for the rf SQUID; for the noise-free case, this has been computed in Ref. 12:

$$\Delta_S(t_0)=-\frac{16}{15}\alpha^2\zeta k+\frac{4\pi Q\Omega^2\sin\Omega t_0}{A_2\sinh[\pi\Omega/(A_2\alpha)^{1/2}]}, \quad (55)$$

where $A_2=0.5928\pi\beta\omega_0^2$. This function, which is peaked at a frequency[12] $\Omega_{Sc}=(1.915/\pi)\sqrt{A_2\alpha}$, is plotted in Fig. 4 for $(\beta,Q,k)=(1.0,4,2.24)$; as in the preceding examples, the straight line represents the first term in (55) and the curve represents the second term (in units of $\sin\Omega t_0$). Introducing the noise term, with noise variance $\sigma^2=0.2$ as before, results in a displacement of the straight line and a shift in the homoclinic threshold; the relative error between the displaced positions of the straight line computed using direct numerical integration of the transport equation, and the WKB solution is about 1.1% for this case.

We complete the analysis by computing the threshold value of Q/k for each of these examples. This is accomplished using the general equations (37) and (38). It is instructive to evaluate this quantity at the critical frequencies Ω_{Dc}, Ω_{Jc}, and Ω_{Sc} at which the curves in Figs. 4–6 are peaked. Using the numerical parameters introduced in this section for each of our model systems we may calculate (at the critical frequency) the parameters (A,B) appearing in Eq. (36) for the new threshold value of Q/k.

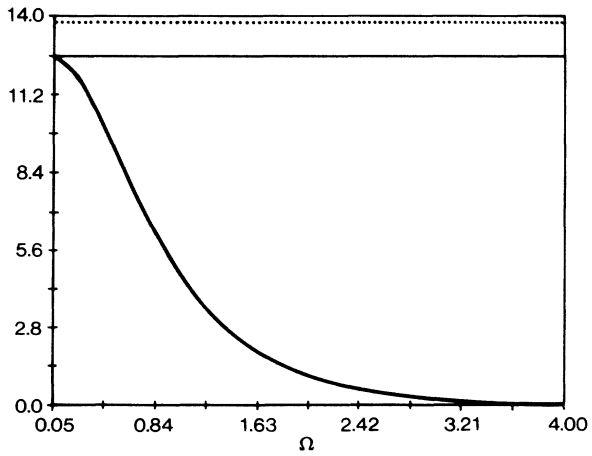

FIG. 3. Melnikov function for the Josephson junction, Eq. (54); same as Fig. 2 with $(Q,k,\sigma^2)\equiv(2.0,1.57,0.2)$.

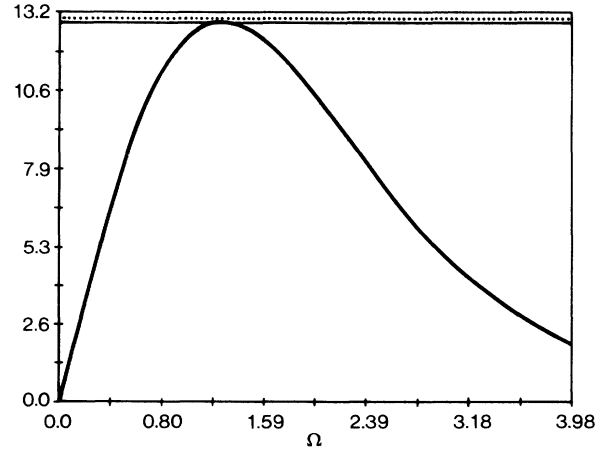

FIG. 4. Melnikov function for the rf SQUID, Eq. (55); same as Fig. 2 with $(\beta,Q,k,\sigma^2)\equiv(1.0,4.0,2.24,0.2)$.

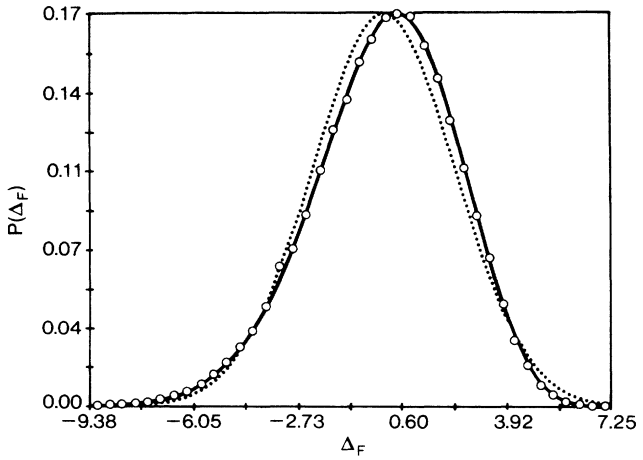

FIG. 5. Probability density function corresponding to the stochastic Melnikov function Δ_F defined in Eq. (7), for the rf SQUID. $(\beta,\omega_0^2,\Omega,Q/k,\sigma^2)\equiv(2.0,1.0,2.0768,4.734,0.8)$. Value of Q/k corresponds to the homoclinic threshold in the absence of noise. Data points represent the result of sampling the Melnikov function with 50 bins. Dotted curve is the Gaussian having the same mean and variance as the sampled data. Solid curve is obtained by assuming "perfect" Gaussian noise (see text).

We find that $(A,B)\equiv(0.71,0.13)$, (1.27,0.31), and (1.78,0.06) for the Duffing oscillator, Josephson junction, and rf SQUID respectively. The relatively small value of B for the rf SQUID is a consequence of our carrying out the analysis in the side well (i.e., along the separatrix z_1z_2) in Fig. 2 rather than in the much deeper center well. This small value of B manifests itself in the relatively small shift in the homoclinic threshold observed for this case (Fig. 4). In the context of the rf SQUID it is interesting to note that the quantity B decreases with increasing β: to produce a given shift in the homoclinic threshold (characterized by the ratio Q/k) requires a larger noise variance as the depth of the well is increased. One expects a similar effect to occur in the other examples (Duffing oscillator and Josephson junction) considered above, as well.

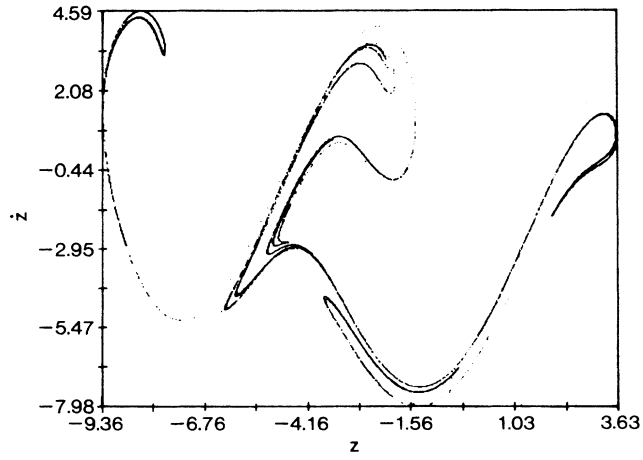

FIG. 6. Poincaré plot of $\dot{z}$ vs z for the rf SQUID with $(\beta,\omega_0^2,\Omega,k,Q)\equiv(2.0,1.0,2.0768,1.1133,10.02)$ in the absence of noise ($\sigma^2=0$).

V. NUMERICAL COMPUTATION OF PROBABILITY DENSITY FUNCTIONS

In this section we consider numerical solutions of the stochastic differential equation for nonlinear dissipative systems driven by random and deterministic (periodic) forces. The stochastic differential equation for such a system may be written in the general form

$$\ddot{x}=k\dot{x}+f(x)=Q\sin\Omega t+F(t)\ , \tag{56}$$

where the parameters k, Q, and Ω as well as the model-dependent nonlinearity function $f(x)$ and the random force $F(t)$ have been defined in the preceding sections. The solution $x(t)$ of (56) is a random variable. Throughout this section, we will consider the effect of a random *initial value,* i.e., the force $F(t)$ is assumed to be a random variable which assumes a new realization at $t=0$ only. Thereafter, it is assumed to remain constant while the equation (56) is integrated. The integration is repeated for several different realizations of the initial value. It is apparent that each new realization of $F(t=0)$ leads to a new potential corresponding to the undriven conservative problem. By requiring the initial value $x(0)$ to correspond to the point z_2 on the potential (see, e.g., Fig. 1) for each integration of (56) we can carry out numerous integrations of this differential equation with each integration corresponding to a different realization of the initial value $x(0)$. Ultimately, the results obtained may be averaged over this ensemble of initial conditions. For the low noise variances of interest in this work, this method yields results that are expected to be fairly close to the results that might be expected if the noise term $F(t)$ was allowed to vary with time throughout the integration of (56).

A comparison of the central theoretical results of this paper to numerical simulation can be made by going back to our basic definition (7) of the stochastic Melnikov function Δ_F and noting that, for a given model system and a specified set of system and driving parameters, one may compute the quantity on the left-hand side of (7) for different realizations of the random force $F(t)$ (taken to have a specified mean and variance). The resulting set of values of Δ_F (we recall that, for each realization of the random term, Δ_F represents the separation of the stable and unstable solution manifolds of the perturbed system) follows a distribution that may be characterized by a probability density function $P(\Delta_F)$. The theory presented in this work predicts that this distribution yields a mean value $\langle\Delta_F(t_0)\rangle$ defined in Eq. (9). The result of a simulation of this probability density function appears in Fig. 5 for the rf SQUID discussed in Sec. IV. We consider, once again, the $\beta=2$ case in the side well (i.e., the separatrix z_1z_2 of Fig. 1). it is assumed that the system is initially at its noise-free homoclinic threshold [$\Delta(t_0)=0$ in (9)] corresponding to values

$(Q/k,\Omega)\equiv(4.734,2.0768)$.

The random noise term is taken to have zero mean and variance $\sigma^2=0.8$ at time $t=0$, as mentioned earlier. This initial value remains unchanged throughout the subsequent integration of (56). For each such realization of the random force, the solution $x(t)$ of the stochastic differential equation (56) and the corresponding realization Δ_F of the stochastic Melnikov function are computed. This is repeated for 75 000 realizations of the random noise term and a distribution function numerically fitted to the results. The computations have been performed on an Apollo DN3500 workstation. For this case, the theory of this paper [Eqs. (9), (10), and (32)] predicts a mean value $\langle\Delta_F\rangle=-0.110$ [since the random force has zero mean, we recall that this value depends only on the third term on the right-hand side of (10)]. In Fig. 5, we show the results of our simulation of the Melnikov function. The probability density function $P(\Delta_F)$ is plotted as a function of Δ_F. The data points represent the probability density function obtained by sorting the 75 000 realizations of Δ_F into 50 bins. This probability density function yields a mean value $\langle\Delta_F\rangle=-0.125$, which is in excellent agreement with the above-mentioned theoretical prediction for this case. The dotted curve in Fig. 5 represents the Gaussian computed with the same mean and variance as our simulated values of Δ_F. It should be noted that this mean value has been computed for the total change in Δ_F. Theoretically, the value of only the first term in Eq. (7) should change in the presence of noise having zero mean value as is the case under consideration. The accurate numerical calculation of the second term in (7) is more difficult than the calculation of the first term; such a numerical calculation yields a very small change in the second term of (7). If one assumes that the second term in (7) does not change (in accordance with the theory), then the probability density function yields a mean value $\langle\Delta_F\rangle=-0.155$. The third (solid) curve in Fig. 5 is obtained as follows: 1000 realizations of Δ_F are calculated for a set of 1000 evenly spaced forces about the zero mean. Each resulting Δ_F is assigned the corresponding probability of the force under a Gaussian distribution (i.e., perfect Gaussian noise, with given variance σ^2 is assumed). $P(\Delta_F)$ is then obtained by renormalization based on the spacing of the Δ_F. It is seen that the results obtained are in excellent agreement (the mean value of Δ_F is the same to the third decimal place) with the data points. The obvious advantage of using this procedure is that a substantially smaller amount of computer time is necessary to achieve accurate results due to the small number (1000) of realizations of F required.

The noise-induced shifts in the Melnikov function are more easily examined in light of Eq. (36). The coefficient B in (36) determines how the homoclinic threshold condition changes in the presence of noise. For the parameters under consideration, Eq. (38a) yields a value of $B=0.025$, using the theory of Sec. III. The numerical simulation (using the method employed to obtain the dotted line in Fig. 4) has been performed for $\sigma^2=0$, 0.4, 0.6, and 0.8. Each of the resulting threshold values Q/k for the four values of σ^2 falls on the same line [represented by Eq. (36)] to within 0.1%. The value of the slope is $B=0.025$ and 0.032 for the cases where, respectively, the total calculated shift, and the shift due to the change in the first term of (7) only, are considered. It is seen that these values agree quite well with the theoretical prediction.

We now return to Eq. (56) and note that, in general, one may construct[25] a two-dimensional Fokker-Planck equation for the complete probability density function $P(x,\dot{x},t|x_0,\dot{x}_0,t_0)$ corresponding to the random variable $x(t)$. The reduced equilibrium distribution function corresponding to the displacement variable x may be formally expressed in the form (up to a normalization constant)

$$P(x)=e^{-\Phi(x)}\ , \tag{57}$$

in terms of a generalized potential function $\Phi(x)$. In general, one cannot analytically compute the function $\Phi(x)$ except in certain approximate cases.[29,30] It has been suggested[29] that when the parameters (k,Q,Ω) in (56) are set so that the system is below its homoclinic threshold then the potential function Φ is a well-behaved differentiable function and has all the properties of a thermodynamic potential. However, when the system (56) is above its homoclinic threshold, the separatrix is no longer continuous and one obtains (as pointed out in Sec. I) an infinity of intersections of the stable and unstable solution manifolds. In this case, it has been suggested[19,29] that the potential function Φ may be nondifferentiable hence one is lead to infer that the occurrence of zeros in the Melnikov function implies that the potential Φ will be nondifferentiable. Further, Jauslin has shown[31] that any nonsingular perturbation of the form $h(x)\sin\Omega(t+t_0)$ will cause the Melnikov function to have simple zeros.

The long-time probability density function defined in (57) is now computed, numerically, for the rf SQUID. A random number generator is used to produce 40 000 realizations of the random noise $F(t=0)$ having zero mean and specified (nonzero) variance σ^2. For each of these realizations, the solution $(z,\dot{z})$ of the differential equation (56) is obtained at a fixed time t, z being the transformed variable used in our computations on the rf SQUID in Sec. IV. For each solution run (corresponding to a particular realization of the random force) we start the particle at the point z_2 in Fig. 1 with zero initial velocity. It should be noted that the points z_1 and z_2 in Fig. 1 must be recomputed for each realization of the random forcing term. We consider the system for the parameter set $(\beta,\omega_0^2,k,Q,\Omega)\equiv(2.0,1.0,1.1133,10.02,2.0768)$ corresponding to the occurrence of a chaotic attractor (these values will remain the same throughout the remainder of this work). Figure 6 shows this chaotic attractor for the noise-free case ($\sigma^2=0$). In Fig. 7 we plot the velocity $\dot{z}$ versus the displacement z for the same case ($Q=10.02$) with a finite noise term ($\sigma^2=10^{-5}$). Each point $(\dot{z},z)$ corresponds to a solution of the stochastic differential equation (56), i.e., a state of the system, for a given realization of the random force. The 40 000 solutions on this figure are all computed at $t=90.7625$ (corresponding to 30 Poincaré periods). The effect of increasing the noise ($\sigma^2=0.004$) is clearly evident in Fig. 8; the same number of points (40 000) are used in this figure, but the increased

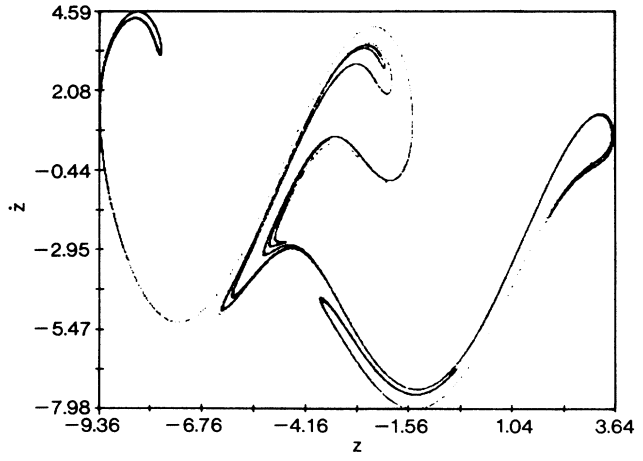

FIG. 7. $\dot{z}$ vs z obtained by solving (56) for the rf SQUID at $t=90.7625$ with $(\beta,\omega_0^2,\Omega,k,Q)$ taking on the same values as Fig. 6. The points correspond to 40 000 realizations of the random force $F(t)$ with zero mean and variance $\sigma^2=10^{-5}$.

noise results in a greater region of phase space being accessible to the system. We note that the deterministic attractor of Fig. 6 could have been obtained in a manner analogous to Figs. 7 and 8 if we had changed the initial condition slightly for each of the 40 000 solutions of the noise-free dynamic equation and computed each solution at the above time $t=90.7625$. In the presence of noise, the potential changes for each realization of the random force and, since we always start the system at the right endpoint z_2 (Fig. 1), we are effectively changing the initial condition for each of the 40 000 solutions. Each realization of the noise (i.e., each realization of the potential) leads to a different region of phase space, i.e., a different attractor that is accessible to the system. Accordingly, the net result in Figs. 7 and 8 is a map that is the *image* of the original (noise-free) attractor. This also explains why the system appears to traverse a greater area of phase space as the noise variance is increased. It must be pointed out that the maps in Figs. 7 and 8, while resembling the deterministic attractor of Fig. 6, do not display the self-replication property that is a hallmark of chaotic attractors; this is evident in Figs. 9(a) and 9(b) in which we show a magnified segment of the deterministic chaotic attractor of Fig. 6 and the corresponding segment from its noisy analog of Fig. 7 ($\sigma^2=10^{-5}$). The self-replication property of the deterministic attractor has been destroyed by the noise. In the limit of even smaller noise variances, one would expect that the phase-space mapping resembles the noise-free chaotic attractor more closely. However, the self-replication property would still be absent in this limit, albeit on a much smaller scale than in Figs. 9(a) and 9(b).

The probability density functions corresponding to the displacement z are plotted in Fig. 10 for the cases $\sigma^2=0$ and 0.04. These probability density functions are equivalent to those that would be obtained from a long-time solution of the Fokker-Planck equation corresponding to the nonlinear system (56). In each case, the proba-

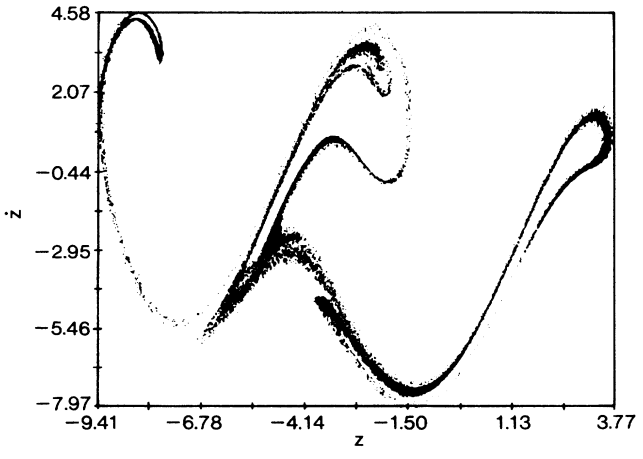

FIG. 8. Same as Fig. 7 with $\sigma^2=0.04$.

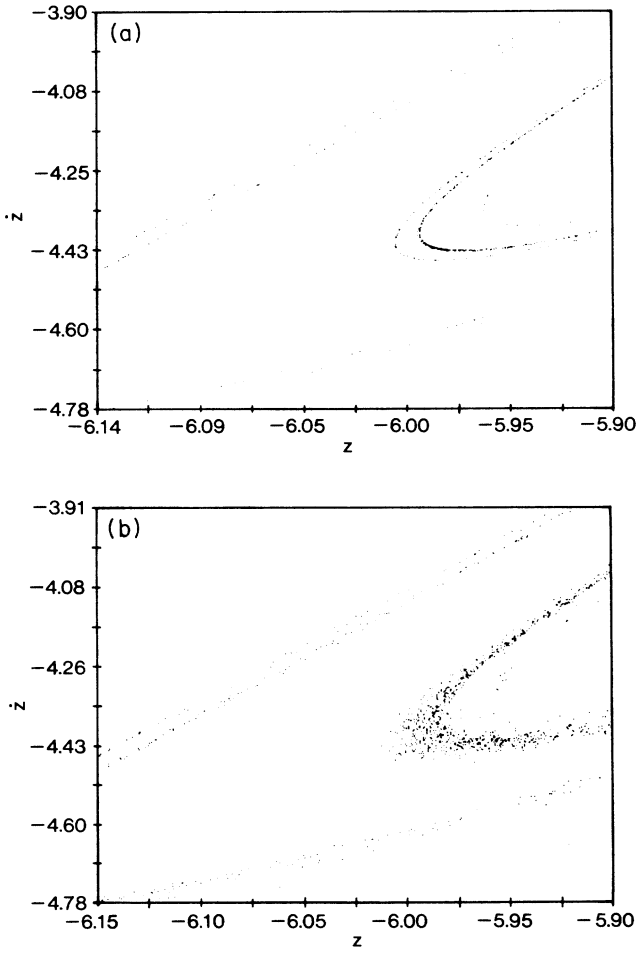

FIG. 9. (a) Magnified section of the chaotic attractor of Fig. 5; the self-replication property is evident. (b) Magnified section of the phase space plot of Fig. 7. There is no self-replication in the presence of even a small amount of noise.

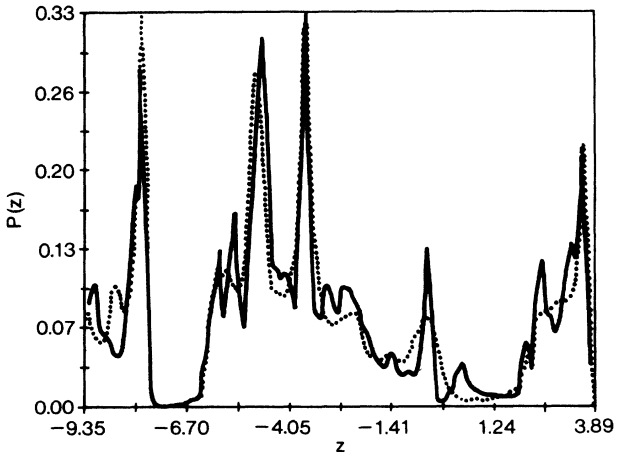

FIG. 10. Probability density function $P(z)$ (solid curve) corresponding to the displacement variable $z(t)$ of Fig. 6. The dotted curve shows the probability density function $P(z,t=90.7625)$ corresponding to the variable z of Fig. 8.

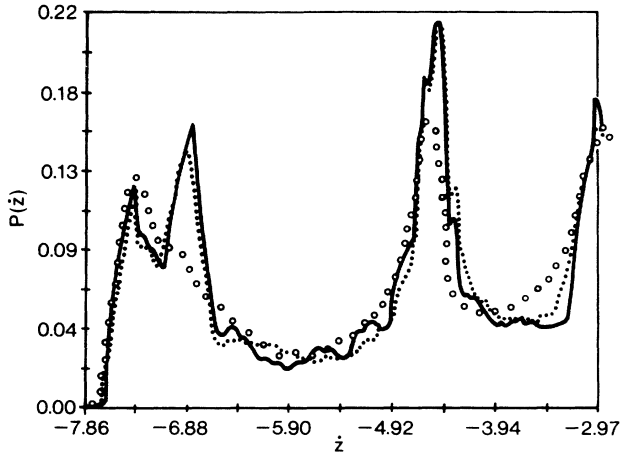

FIG. 12. Velocity probability density functions; same as in Fig. 11. The range of velocities $\dot{z}$ corresponds to the displacement range of Fig. 11.

bility density function is seen to display multiple maxima, reminiscent of the nondifferentiable potentials suggested by Kapitaniak[19] and Graham and Tel.[29] The probability density function is a measure of the frequency with which each elemental area of phase space is traversed by the system. In the presence of noise, the peaks in the probability function maxima are seen to have a greater width but a smaller height than those corresponding to the noise-free case; the noise tends to "smooth" the probability density function coarse graining the deterministic "randomness" of the attractor itself. This effect is a direct consequence of the greater region of phase space that is made available to the system in the presence of noise (we recall that the same number of points, 40 000, appear in Figs. 6–8). A similar effect is evident if we consider the probability density functions corresponding to the velocity variable. Finally, we show (in Fig. 11) a small section of the displacement probability density function $P(z)$ for the cases $\sigma^2=0$, 10^{-5}, and 0.04. The smoothing effect of the noise is evident in this figure as well as in Fig. 12 in which we plot the velocity probability density function for the range of velocities corresponding to the displacements (horizontal scale) of Fig. 11.

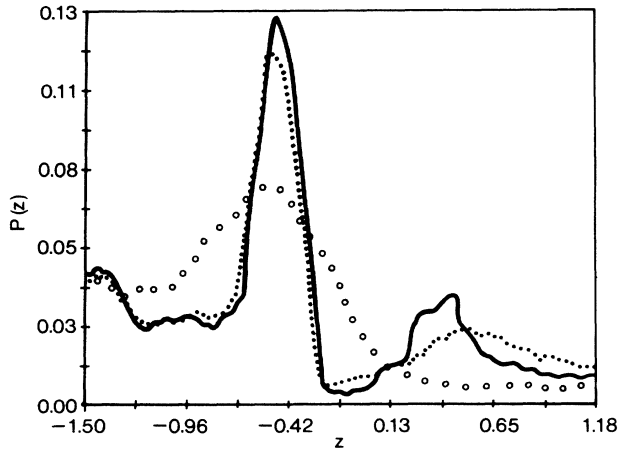

FIG. 11. Displacement probability density functions magnified over a very small range of the displacement. Solid curve represents $P(z)$ corresponding to the attractor of Fig. 6, dotted curve represents $P(z,t=90.7625)$ corresponding to the noisy case of Fig. 7, and data points represent the case of Fig. 8. The smoothing effect of the noise is evident.

VI. DISCUSSION

In this work, we have presented a theory that predicts that the presence of weak Langevin noise in a dissipative nonlinear system suppresses, in the mean, homoclinic behavior that might normally be observed in the noise-free system. This result is in agreement with the work of Carlson[23–24] and Schieve and Petrosky[21–22] on the effect of quantum fluctuations on the homoclinic threshold in driven dissipative classical systems. We have introduced a generalization of the Melnikov function in the presence of the external noise. This function is stochastic, but by averaging it over the ensemble of the noise, one obtains an averaged Melnikov function that corresponds to its noise-free analog shifted by a constant correction term.

The significance of this generalized Melnikov function is worth some further discussion. It is well known[2–6] that, in a noise-free nonlinear dynamic system the zeros of the Melnikov function are associated with homoclinic tangencies and chaos via horseshoes; the Melnikov method for this case is applicable to small perturbations of the separatrix motion. In Secs. II and III above, we have assumed that the Langevin noise is weak enough that the deviations from the separatrix motion for each separate realization of the random force term $F(t)$ in (1) are very small, i.e., the second term in (4) is quite small compared to the term $x_s(t)$, which represent the separatrix solution for the noise-free case. It is further assumed that the averaged motion coincides with the separatrix of the noise-free problem, i.e., $\langle \delta x(t) \rangle = 0$ in (5) [this follows directly from our assumption of a zero mean initial condition: $\langle \delta x(t_0) \rangle = 0 = \langle \delta \dot{x}(t_0) \rangle$]. Clearly, the gen-

eralized Melnikov function, being an averaged quantity, represents a deviation from homoclinicity in the mean. The distribution of this Melnikov function (Fig. 5) obtained via numerical simulation is peaked at some mean value $\langle \Delta_F \rangle$. If this distribution were Gaussian, this mean value would correspond to the most probable value of Δ_F which, from Eq. (9), is the noise-free Melnikov function shifted by a small correction term. Figure 5 indicates that the deviation from a Gaussian distribution is small. In fact, for noise variances smaller than the value 0.8 used in this figure, the distribution $P(\Delta_F)$ approximates a Gaussian more closely. Hence, for the low-noise variances required by our perturbation-theoretic arguments of Sec. II, it is reasonable to expect that the probability of observing a homoclinic tangency *in the mean* is a maximum for the parameters which determine the zeros of the Melnikov function in the noise-free problem. In fact, in this limiting case of a very low noise, one may (assuming the distribution of Δ_F shown in Fig. 5 to be approximately Gaussian) write down an analytical expression for the probability density function that characterizes Δ_F:

$$P(\Delta_F) \approx (2\pi\sigma_F^2)^{-1/2} \exp\left[-\frac{(\Delta_F - \langle \Delta_F \rangle)^2}{2\sigma_F^2} \right],$$

σ_F^2 being the variance of Δ_F and $\langle \Delta_F \rangle$ being the mean value which is defined in Eq. (9) and may be determined directly from numerical simulations as described in Sec. V. For a given realization of the noise, the probability that Δ_F vanishes may be deduced directly from the above expression. This allows one to compute the probability that a given realization of the noise will result in a homoclinic tangency. In the limit of vanishing noise, the distribution $P(\Delta_F)$ will be very sharply peaked (approaching a δ function) at its noise-free value $\Delta(t_0)$. For finite small noise, each realization of the noise leads, in general, to a separation of the stable and unstable manifolds given by the stochastic quantity of Eq. (8); this separation is offset from its noise-free value. The comments of this paragraph, and the results embodied in Eqs. (8) and (9) might be directly verified by plotting the stable and unstable solution manifolds for a given model system (see, e.g., Refs. 4, 5, and 12) for numerous realizations of the random noise. Such a simulation would be costly, but possibly feasible.

The correction term $\langle \Delta_c \rangle$ of Eq. (9) has been estimated (within the limits of accuracy of the WKB approximation) using the procedure described in Sec. III. In this context we must point out that better accuracy may be obtained by retaining higher-order terms in the WKB expansion [the solutions (22) and (29) represent only the first-order solutions, the so-called "physical optics approximation"]. However, although the agreement between the solutions obtained using this approximation and those obtained via a direct numerical solution of the transport equation (13) may not be perfect, we find that the correction to the Melnikov function calculated using the *integral* of the square of the solution is almost the same using the two procedures. Our analysis has taken into account the case in which the Langevin noise has zero mean value as well as the case in which this mean value is finite. In the former case, the mean displacement $\langle x(t) \rangle$ as well as the associated mean velocity $\langle \dot{x}(t) \rangle$ of the noisy unperturbed system follow the separatrix motion of the corresponding noise-free system, through our choice of zero initial values in the solution of the transport equation (13). This ensures that the Melnikov correction term depends solely on the second-order statistics [in this case the initial variance $\langle \delta\dot{x}^2(0) \rangle$] of the random variable $\langle \delta\dot{x}(t) \rangle$. However, if we choose a nonzero initial condition, then the expression (10) contains contributions from all the terms on the right-hand side even if the noise term has zero mean value. The case in which the noise has a finite mean value has also been considered. In this case, the first two terms on the right-hand side of (10) contribute to the correction term (regardless of whether we assume a vanishing initial condition or not). It is seen that the presence of a finite mean value does not lower the homoclinic threshold. In this context it is worth pointing out that weak multiplicative fluctuations in the nonlinearity parameter of a driven dissipative system may, on average, *lower* the homoclinic threshold.[32]

By expressing the initial variance $\langle \delta\dot{x}^2(0) \rangle$ in terms of the variance of the noise, we have been able to quantify the assumption of weak Langevin noise [our value $\sigma^2 = 0.2$ of the external noise variance used in the numerical calculations corresponds to an initial velocity variance $\langle \delta\dot{x}^2(0) \rangle = 0.1$, which agrees with our definition of weak noise introduced in Sec. III]. The implementation of this assumption within the framework of the perturbation theory that underlies the Melnikov function, leads one to believe that the calculation of the noise-induced shift in the Melnikov function is very accurate (the correspondence with a real system is likely to improve if one assumes even weaker noise, i.e., if both m and σ^2 are reduced even further). This idea is further strengthened by the results of our numerical computations of the probability density function $P(\Delta_F)$ in Sec. V; these computations yield values of the mean $\langle \Delta_F \rangle$ that agree very well with those computed using the theory of Sec. III despite the fact that the computations of this section were carried out using a random initial value and then assuming the noise to be constant throughout the remainder of each integration of the stochastic differential equation (56). Increasing the noise variance elevates the homoclinic threshold. Since noise is present in most real experiments, one must conclude that some results of experiments carried out on deterministic nonlinear systems might well be chaotic were it not for the smoothing effect of the system noise. The numerical work of Sec. V, summarized in Figs. 6–12 displays this smoothing effect [we reiterate that these results were obtained using a random dc driving in the stochastic differential equation (56)] on the multimaximum probability density functions that characterize the chaotic regime.

ACKNOWLEDGMENTS

One of us (A.R.B.) would like to acknowledge support from the office of Naval Research under Grant No. N0001489AF00001.

[1]H. Poincaré, *New Methods of Celestial Mechanics* (Gauthier-Villars, Paris, 1899), Vol. 3, p. 391.
[2]J. Moser, *Stable and Random Motions* (Princeton University Press, Princeton, 1973).
[3]V. Melnikov, Trans. Moscow Math. Soc. **12**, 1 (1963).
[4]P. Holmes, Philos. Trans R. Soc. London Ser. A **292**, 419 (1979).
[5]J. Guckenheimer and P. Holmes, *Nonlinear Oscillations, Dynamical Systems and Bifurcations of Vector Fields* (Springer-Verlag, New York, 1983).
[6]V. Arnold, Dokl. Akad. Nauk SSSR **156**, 9 (1964) [Sov. Phys. Dokl. **5**, 581 (1964)].
[7]J. Sanders, Celest. Mech. **28**, 171 (1982).
[8]R. Kautz and R. Monaco, J. Appl. Phys. **57**, 875 (1985).
[9]R. Kautz and J. Macfarlane, Phys. Rev. A **33**, 498 (1986).
[10]Z. Genchev, Z. Ivanov, and B. Todorov, IEEE Trans. Circuits Syst. **CAS-30**, 633 (1983).
[11]V. Gubankov, S. Zyglin, K. Konstantinyan, V. Koshelets, and G. Ovsyannikov, Zh. Eksp. Teor. Fiz. **86**, 343 (1984) [Sov. Phys.—JETP **59**, 198 (1984)].
[12]W. Schieve, A. Bulsara, and E. Jacobs, Phys. Rev. A **37**, 3541 (1988).
[13]J. Cruthfield, J. D. Farmer, and B. Huberman, Phys. Rep. **92**, 45 (1982).
[14]H. Svensmark and M. Samuelson, Phys. Rev. A **36**, 2413 (1987).
[15]K. Wiesenfeld and B. McNamara, Phys. Rev. Lett. **55**, 10 (1985).
[16]K. Wiesenfield and B. McNamara, Phys. Rev. A **33**, 629 (1986).
[17]F. Arecchi, R. Badii, and A. Politi, Phys. Rev. A **32**, 402 (1985).
[18]R. Kautz, Phys. Rev. A **38**, 2066 (1988).
[19]T. Kapitaniak, *Chaos in Systems with Noise* (World Scientific, New York, 1988).
[20]K. Matsumoto and I. Tsuda, J. Stat. Phys. **31**, 87 (1983).
[21]W. Schieve and T. Petrosky, in *Quantum Optics IV,* edited by J. Harvey and D. Walls (Springer-Verlag, New York, 1986).
[22]T. Petrosky and W. Schieve, Phys. Rev. A **31**, 3907 (1985).
[23]L. Carlson, Ph.D. thesis, University of Texas, 1989.
[24]L. Carlson and W. Schieve, J. Math. Phys. (to be published).
[25]H. Risken, *The Fokker Planck Equation* (Springer-Verlag, New York, 1989).
[26]N. van Kampen, *Stochastic Processes in Physics and Chemistry* (North-Holland, Amsterdam, 1983).
[27]R. Langer, Bull. Am. Math. Soc. **40**, 545 (1934).
[28]R. Barone and G. Paterno, *Physics and Applications of the Josephson Effect* (Wiley, New York, 1982).
[29]R. Graham and T. Tel, J. Stat. Phys. **35**, 729 (1984).
[30]R. Graham and T. Tel, Phys. Rev. A **31**, 1109 (1985).
[31]H. Jauslin, J. Stat. Phys. **42**, 573 (1986).
[32]W. C. Schieve and A. R. Bulsara, Phys. Rev. A (to be published).